Proceedings of the
Symposium on Radon
Reduction Technology
Denver, CO, 10/88

RADON DIAGNOSTICS: SUBSLAB COMMUNICATION AND PERMEABILITY MEASUREMENTS

T. G. Matthews, D. L. Wilson, P. K. TerKonda, R. J. Saultz,
G. Goolsby, S. E. Burns and J. W. Haas
Measurement Systems Research Group
Health and Safety Research Division
Oak Ridge National Laboratory,
Oak Ridge, TN 37831

*Research sponsored jointly by the Environmental Protection Agency (IAG-40-1709-85), the Tennessee Valley Authority (IAG-40-1710-1710-10), and the U.S. Department of Energy under contract DE-AC05-84OR21400 with Martin Marietta Energy Systems, Inc. This work has not been subject to the EPA's peer and administrative review and, therefore, does not necessarily reflect the views of the Agency and no official endorsement should be inferred.

Abstract

Mathematical models are developed from Darcy's Law to determine the intrinsic permeability of soil and subslab soil/gravel media. Three geometrical configurations have been applied as boundary conditions: a spherical geometry for soil tube measurements, a hemispherical geometry for subslab measurements in the absence of a gravel layer, and a cylindrical disk geometry for subslab measurements in the presence of a gravel layer. A power dependence on pressure is included in all three models to investigate potential nonlaminar air flows. The results of extensive permeability studies at six Tennessee Valley homes are fit to the models using non-linear regression analysis. All three models yield an average exponent of about 0.7 for the pressure term, indicating some degree of nonlaminar flow. Less than proportionate increases in mitigation effectiveness with increased blower capacity are predicted in subslab ventilation systems. Subslab permeabilities and induced pressure field radii are almost always increased by installation of gravel-filled pits as part of the subslab ventilation system. In a house with no pre-existing subslab gravel layer, order of magnitude increases in permeability and extensions in pressure field radii were observed. The subslab permeability at selected sites in this house also exhibited a strong depth dependence because of hard clay and soil layers within the first 150 cm beneath the slab. In houses with pre-existing subslab gravel layers, installation of mitigation pits resulted in no change to 3 fold increases in permeability and extensions in induced pressure field radii. These findings are supported by the mathematical forms of the hemispherical and cylindrical disk models.

Introduction

Radon 'diagnostic' measurements are an integral component in understanding radon entry into buildings, and in the design and implementation of effective radon control systems (1). For homes with basement or slab on grade construction, subslab 'communication' measurements are used to evaluate the permeability of the soil/gravel mixture beneath the slab and the extension of induced 'pressure fields' beneath the slab from individual or multiple suction points (1, 2). An improved understanding of the principles that

govern pressure-induced flow of air beneath concrete slabs is needed. This will enhance our use of radon diagnostic techniques and the effectiveness of engineering measures that are implemented to control indoor radon, particularly under conditions of low permeability beneath the slab.

Darcy's Law is used to describe laminar flow of air through porous media,

$$V = - K \, dp/dx \qquad (1)$$

where x refers to the average direction of flow, V is the mean velocity (cm/sec), dp/dx is the change in piezometric pressure per unit distance in the x direction (i.e., the pressure gradient, cm H_2O/cm), and K is the conductivity of a fluid (i.e., air) in a porous medium per unit gradient [(cm/sec)/(cm H_2O/cm)] (3). The piezometric pressure, p, is the sum of the potential energy (i.e., elevation head) and pressure head for the fluid at a given location. The potential energy is assumed to be zero because all measurements are performed at essentially the same datum plane (i.e., reference elevation).

The intrinsic permeability, k [(cm^2) per (cm H_2O/cm)], is defined as

$$k = K \, \mu \, / \, \rho \, g \qquad (2)$$

where μ is the dynamic viscosity [g/(cm sec)], ρ is the fluid density (g/cm^3), and g is the acceleration due to gravity (cm/sec^2) (4). Substituting for K in Equation 1,

$$V = - (k \, \rho \, g \, / \, \mu) \, dp/dx \qquad (3)$$

In order to remove dimensional units from p for further model development, let

$$p' = p \, / \, p_{std} \qquad (4)$$

where p is in units of cm H_2O and p_{std} is 1 cm H_2O. Rearranging Equation 4 and differentiating,

$$dp = p_{std}\, dp' \tag{5}$$

Substituting Equation 5 into Equation 3,

$$V = -\left(k\, \rho\, g\, p_{std} / \mu \right) dp'/dx \tag{6}$$

A semi-empirical modification of Darcy's Law is considered to account for anticipated deviations from laminar flow in radon diagnostic studies of soil and soil/gravel mixtures. Such deviations have been hypothesized in diagnostic measurements of soil permeability (5). The dependence of velocity on the gradient dp/dx is modeled with an exponent 'b' for the pressure term, p', in Equation 6. The validity of this simplifying assumption will be examined in future studies.

$$V = -\left(k\, \rho\, g\, p_{std} / \mu \right) dp'^{b}/dx \tag{7}$$

Similar modifications to Darcy's Law have been proposed for studies of non-laminar flow of fluids in porous media (6). A quadratic dependence on pressure (i.e., $p^{0.5}$) is anticipated for turbulent flows.

The velocity term, V, in Darcy's Law is normally expressed as the flow rate of the fluid, Q (cm^3/sec), per unit cross-sectional area, A (cm^2). Substituting into Equation 7,

$$Q / A = -\left(k\, \rho\, g\, p_{std} / \mu \right) dp'^{b}/dx \tag{8}$$

Three models are considered to describe pressure- or vacuum-induced flow in porous soil and soil/gravel mixtures. These models are proposed to bound the modified Darcy's Law (i.e., Equation 4) for common radon diagnostic applications to measure intrinsic permeability. A spherical model has previously been used to describe pressure-induced flow radially in all directions from the end of a tube extending approximately one meter into the soil (2). Rearranging Equation 8,

$$(Q\ \mu)/(4\ \pi\ r^2\ \rho\ g\ p_{std}) = -\ k\ dp'^{b}/dr \qquad (9)$$

where $4\pi r^2$ is the spherical surface area, A.

Two additional models are presented to describe vacuum-induced flow beneath a concrete slab. A hemispherical model assumes uniform flow from all hemispherically bounded directions towards the point of penetration (e.g., suction point) through the slab,

$$(Q\ \mu)/(2\ \pi\ r^2\ \rho\ g\ p_{std}) = -\ k\ dp'^{b}/dr \qquad (10)$$

where $2\pi r^2$ is the hemispherical surface area. The hemispherical model is considered for porous soil beneath a concrete slab in the absence of a gravel layer.

A cylindrical disk model assumes uniform flow from all areas of the band surrounding the edge of a cylinder towards the point of penetration through the slab

$$(Q\ \mu)/(2\ \pi\ r\ h\ \rho\ g\ p_{std}) = -\ k\ dp'^{b}/dr \qquad (11)$$

where h is the thickness (cm) of the disk. The cylindrical disk model is considered for a permeable gravel layer beneath a concrete slab. No air flow is considered from the bottom of the disk, that is, from the comparatively impermeable soils beneath the gravel.

All models are integrated from the point of penetration of the soil or slab (i.e., at $r = r_o$, $p' = p'_o$) to the outer fringe of induced differential pressure field (i.e., at $r = r_x$, $p' = p'_x$) in the porous medium. The following expressions are determined:

$$-1/r_x + 1/r_o = -\ [4\ \pi\ k\ \rho\ g\ p_{std}\ /\ Q\ \mu\ (1+b)]\ (p'^{1+b}_x - p'^{1+b}_o) \qquad (12)$$

for the spherical model,

$$-1/r_x + 1/r_o = -\ [2\ \pi\ k\ \rho\ g\ p_{std}\ /\ Q\ \mu\ (1+b)]\ (p'^{1+b}_x - p'^{1+b}_o) \qquad (13)$$

for the hemispherical model, and

$$\ln (r_x/r_o) = - [2 \pi k \rho g h p_{std} / Q \mu (1+b)] (p'^{1+b}_x - p'^{1+b}_o) \qquad (14)$$

for the cylindrical disk model.

Several simplifying assumptions are then made. In all models, the pressure (i.e., the induced pressure above or below atmospheric pressure) at p'_x is assumed to be zero. For the spherical and hemispherical models $1/r_o$ is much larger than $1/r_x$ for moderately permeable media, therefore, $1/r_x$ is set equal to zero. The term, $\ln r_x/r_o$, in the cylindrical disk model is treated as a constant, R, which is insensitive to typical variations in r_x and r_o. For example, R varies from 4 to 7 for 3.8 cm ID penetrations of a slab (i.e., r_o = 1.9 cm) and pressure field radii (i.e., r_x) varying from 100 cm (i.e., low permeability soils) to 2100 cm (i.e., permeable gravel). An R value of 6 $\pm$ 1, corresponding to a r_x value of 760 cm and range of r_x values from 280 to 2100 cm, is suggested for most premitigation diagnostic applications in the absence of pressure field mapping data to determine r_x. Applying the same assumptions, R values of 5 $\pm$ 1 and 4.6 $\pm$ 1 are suggested for 10 cm and 15 cm ID penetrations of a slab. In all three models the absolute (i.e., positive) value of p'_o is used for both pressurized and depressurized conditions to avoid algebraic sign problems.

The simplified expressions are

$$1/r_o = [4 \pi k \rho g p_{std} / Q \mu (1+b)] (|p'_o|^{1+b}) \qquad (15)$$

for the spherical model,

$$1/r_o = [2 \pi k \rho g p_{std} / Q \mu (1+b)] (|p'_o|^{1+b}) \qquad (16)$$

for the hemispherical model, and

$$R = [2 \pi k h \rho g p_{std} / Q \mu (1+b)] (|p'_o|^{1+b}) \qquad (17)$$

for the cylindrical disk model.

Rearranging, performing unit conversions, and substituting 980.7 cm/sec^2 for g, 1.2×10^{-3} g/cm^3 for ρ, and 1.8×10^{-4} g/(cm sec) for μ in Equations 15 to 17, the intrinsic permeability, k [(cm^2) per (cm H_2O/cm), is given as

$$k = 2.0 \times 10^{-4} \, Q \, (1+b) \, / \, (r_o \, p_{std} \, |p'_o|^{1+b}) \qquad (18)$$

for the spherical model,

$$k = 4.1 \times 10^{-4} \, Q \, (1+b) \, / \, (r_o \, p_{std} \, |p'_o|^{1+b}) \qquad (19)$$

for the hemispherical model, and

$$k = 4.1 \times 10^{-4} \, Q \, R \, (1+b) \, / \, (h \, p_{std} \, |p'_o|^{1+b}) \qquad (20)$$

for the cylindrical disk model, where the constant (i.e., conversion factor) has units of cm^4 min/L, and

Q = flow (L/min),
r_o = radius (cm)
p' = dimensionless parameter equal to p/p_{std},
p_{std} = 1 cm H_2O, and
h = height of the subslab gravel layer (cm).

Rearranging Equations 19 and 20 to solve for flow [i.e., Q (L/min)], the above models can be used to propose techniques to improve subslab communication. Q in the hemispherical model is proportional to k, r_o, and $p'_o{}^{1+b}$. Hence,

$$Q = 2.4 \times 10^{3} \, k \, r_o \, p_{std} \, |p'_o|^{1+b} \, / \, (1+b) \qquad (21)$$

For the cylindrical disk model Q is proportional to k, h, $p'_o{}^{1+b}$ and 1/R (i.e., ln r_o/r_x). Hence,

$$Q = 2.4 \times 10^{3} \, k \, h \, p_{std} \, |p'_o|^{1+b} \, / \, (R \, (1+b)) \qquad (22)$$

The subslab intrinsic permeability, k, and the height of gravel layer beneath the concrete slab, h, cannot be easily modified. For both models $p'_o{}^{1+b}$ is affected by blower capacity. For the hemispherical model, increasing r_o, the radius of the hemispherical hole beneath the slab, should improve subslab communication. Therefore, in the absence of a subslab gravel layer the installation of gravel-filled pits is anticipated to increase the air flow and extend the induced pressure field beneath the concrete slab. In contrast, in the presence of a subslab gravel layer much smaller improvements in subslab communication are anticipated with the installation of gravel pits; Q is insensitive to variations in r_o in the cylindrical disk model.

Investigations of soil and subslab permeability and pressure field extension beneath slabs, plus the analysis of these data using the above models are described below. These studies have occurred as part of a detailed investigation of radon entry and control in four 'basement rancher' homes in Oak Ridge, TN and two 'raised rancher' homes in Huntsville, AL, that contain both crawlspace and garage/basement areas (7).

Experimental Procedures

Basic Study Design: Four homes were selected in both Oak Ridge, TN, and Huntsville, AL, for detailed study of radon entry and control in indoor environments. Study houses in each city were similar in house construction characteristics, heating/cooling system design, and indoor radon concentrations. The homes were also tightly clustered for purposes of geologic and meteorologic homogeneity (see Table 1). Houses 15-18 in Oak Ridge, TN, and Houses 13 and 14 in Huntsville, AL, had concrete slabs in basement and garage areas, respectively.

Soil Permeability Measurements: Soil permeability measurements were performed at least once per season in the soil surrounding typically three or four sides of each study home. The permeability was measured from the end of a soil tube (1 cm ID) driven approximately one meter into the ground and located approximately 1-2 meters from the side of the house. All soil tubes were capped except during measurement periods. Permeability was determined using a pressurized air cylinder, calibrated rotameters to measure air flow into the

ground, and an electronic vacuum sensor to measure differential pressure at the end of the soil tube. Each determination of soil permeability consisted of several measurements taken at typically 5-10 different air flows and pressures.

Subslab Permeability and Pressure Field Mapping: Subslab communication measurements were performed in both pre- and post-mitigation phases of the study in Houses 13-18. The communication tests included measurements of subslab permeability and the mapping of induced pressure fields beneath the slab (see the data acquisition form given in Table 2 for subsequent discussion). The subslab permeability was typically determined by applying negative pressure to a hole in the slab and measuring the flow of exhausted air. Permeabilities were often measured over a 10 to 100 fold range of pressures and air flows at each hole. In the premitigation diagnostic phase, suction was applied with a variable speed shop vacuum to a 3.8 cm ID hole in the slab. Air flow was measured with a hotwire anemometer inserted into a 2.6 cm ID PVC exhaust pipe. In several homes, the permeabilities of the subslab soil and soil/gravel mixtures were investigated as a function of depth by coring the 2.6 ID holes to various depths of approximately 10, 40, 80 and 120 cm. In the postmitigation phase, suction was applied with a variable speed mitigation blower through 10.2 and 15.2 cm holes in the slab. These holes connected directly to 50 x 50 cm gravel-filled pits having typically 40 and 150 cm depths for homes with and without subslab gravel layers, respectively. Air flow was monitored with a hotwire anemometer inserted into a 13.9 or 15.2 cm ID exhaust pipe. In both pre- and post-mitigation phases, the induced differential pressure was monitored at the point of entry into the slab with an electronic vacuum guage.

Pressure field mapping was accomplished by applying controlled vacuums to premitigation diagnostic holes or postmitigation holes/pits and monitoring the induced pressure through 1 cm ID holes in the slab at remote locations. In the premitigation diagnostic phase, negative pressures of 0.5, 2.0 and 5.0 kPa were used whenever possible to enhance interhouse comparisons, tests of reproducibility between different time periods, and comparisons between pre- and post-mitigation phases of the program. In the postmitigation phase, negative pressures were limited to about 0.35 kPa due to the blower capacity.

Results and Discussion

The results of experimental investigations of permeability in soil, subslabs without a gravel layer, and subslabs with a gravel layer were fitted to the spherical, hemispherical and cylindrical disk models, respectively, using non-linear regression analyses (8). Modeled coefficients consisted of the intrinsic permeability, k, and the power function term, b, in Equations 18-20. The following discussion is broken down into the assignment of numerical values to modeling constants (i.e., r_o, R, h), the modeled results for k and b, and finally, comparisons of these permeability results to extensions of induced pressure fields.

Modeling Constants: The assignment of numerical values to constants in the spherical, hemispherical and cylindrical disk models required detailed consideration of the physical geometry in the soil and subslab experiments. The simplest case was the measurement of soil permeability with outdoor soil tubes. The spherical model (i.e., Equation 15) was used, assuming an r_o of 0.4 cm, the inner radius of the soil tube.

The hemispherical model (i.e., Equation 19) was applied to subslab permeability experiments in the absence of a distinct gravel layer (i.e., < 2 cm thick). This included all subslab measurement locations at house 16 and the work room in House 15 (see Table 3). The radius r_o in Equation 19 was approximated as the radius of a hemisphere with surface area equal to that of the experimental holes beneath the slab. In premitigation tests, for example, the hemispherical r_o was calculated from the following expression,

$$2 \pi r_o^2 = 2 \pi s l + \pi s^2 \qquad (23)$$

where s and l are the radius (i.e., 1.9 cm) and length of the augered tubular holes, respectively. In the postmitigation tests, an effective r_o was calculated for the roughly cylindrical gravel-filled pits of typically 40 or 150 cm depth (see Figure 1).

The cylindrical disk model (i.e., Equation 20) was applied to subslab permeability experiments in the presence of a distinct gravel layer. This included all subslab measurement locations at Houses 13, 14, 17, and 18, plus the outdoor closet at House 15 (see Table 3). The average thickness of the subslab gravel layer (i.e., h in Equation 20) was estimated as 10 cm beneath Houses 13, 14, and 18, 12.5 cm beneath House 17, and 15 cm beneath House 15. The constant R (i.e., ln r_x/r_o) was assumed to be 6 for the premitigation diagnostic experiments (i.e., taken through 3.8 cm ID holes in the slab). The R value was calculated from ln (760 cm/1.9 cm) = 6. An R value of 3.4 was used for all postmitigation permeability measurements [i.e., ln (760 cm/25 cm) = 3.4], where 25 cm is the approximate cylindrical radius of the top of all of the mitigation pits. An arbitrary r_x value of 760 cm was chosen for calculational purposes in the development of the model (see page 6 of the introduction for clarification).

Exponent (1+b) for Pressure Term: An important goal in modeling the permeability data for soil and subslab applications was the empirical determination of the power dependence on pressure (i.e., 1+b in Equations 18-20). The average and standard deviation (i.e., $x_{avg} \pm \sigma$) of the exponent 1+b for 75 soil tube data sets using the spherical model was 0.77 ± 0.20. Applying the hemispherical model, x_{avg} and σ were 0.70 ± 0.27 for 35 premitigation data sets and 0.80 ± 0.20 for 23 postmitigation data sets. Finally, applying the cylindrical disk model, x_{avg} and σ were 0.64 ± 0.13 and 0.66 ± 0.10 for 39 premitigation and 19 postmitigation subslab data sets, respectively. An approximate exponent of 0.7 for the pressure term has at least two important implications. First, it suggests non-laminar and potentially turbulent air flow in both the soil and subslab permeability experiments. Second, it suggests that increased negative pressures in subslab ventilation systems utilizing more powerful blowers will yield less than directly proportionate improvements in air flow. Both the hemispherical and cylindrical disk models (see Equations 21 and 22) predict only a 60 % increase in air flow with twofold increases in negative pressure.

Modeled Subslab Permeabilities: The modeled results for individual data sets of pre- and post-mitigation measurements of subslab permeability are given in Table 3. As previously described, the same models (i.e., hemispherical or cylindrical disk) are used to calculate the intrinsic permeabilities in both pre- and post-mitigation data sets for a given measurement site. The results range from 0.005×10^{-4} to 210×10^{-4} cm^2 in pre-mitigation tests and from 2.8×10^{-4} to 420×10^{-4} cm^2 in postmitigation tests. The installation of gravel-filled pits beneath slabs with a gravel layer caused no change in permeability for Houses 13 and 14, and an approximate two to threefold increase in permeability for Houses 15 (i.e., closet hole), 17 and 18. Increases in permeability might be expected if the mitigation pit enhanced contact with the existent gravel layer. In House 16 (i.e., no subslab gravel layer) approximately eightfold and thirtyfold improvements were observed in the den and laundry areas, respectively. Such increases may be caused by physical differences between the augered diagnostic holes and the excavated mitigation pits. Soils tended to pack inside of the diagnostic holes during the augering process, potentially reducing the permeability. In contrast, the soil was highly fractured during the excavation of 150 cm deep gravel pits, potentially increasing the permeability.

These pre- and post-mitigation comparisons were made possible because of the good to excellent experimental reproducibility that was observed between different time periods. The results for most replicate data sets listed in Table 3 include changes in personnel and temporal separations of weeks to months. This reproducibility is in stark contrast to the 100 to 1000 fold variation in permeability observed in soil tube measurements surrounding the study homes (see Table 3).

The permeability data for a few of the measurement sites, in particular in House 16, demonstrated an interesting dependence on depth below the slab (Table 3). For example, an impermeable clay material was found in the laundry room of House 16 for the first 60-90 cm beneath the slab. The permeability dropped to 5×10^{-7} cm^2 in a 40 cm hole, but increased to $6\text{-}7 \times 10^{-5}$ cm^2 in more permeable, granular soils encountered at depths greater than 110 cm beneath the slab. In contrast, uniformly low permeabilities were observed in the den with increasing depth. In the bedroom, the permeability gradually

declined with depth. This most likely indicates that the more permeable soils were layered just beneath the slab.

The selection of the hemisphere versus the cylindrical disk model for individual measurement sites depended on the presence or absence of a subslab gravel layer. This selection had a significant impact on the calculated permeabilities, particularly with the postmitigation data. For example, the premitigation permeabilities for Houses 13, 14, 17, 18, and the outdoor closet of House 15 were on average two to fourfold higher when calculated using the cylindrical disk model as opposed to the hemispherical model. In contrast, the postmitigation permeabilities for the same houses were 15 to 20 fold higher using the cylindrical disk model. Intermodel variations were much larger for House 16 (which contained no subslab gravel layer) because the cylindrical disk model (i.e., Equation 20) became unstable as the thickness of the gravel in the denominator approached zero. These intermodel variations are caused by the mathematical form of the models and their constants, which must be carefully considered in future applications. The cylindrical disk model has a reduced cross-sectional area for air flow (i.e., the outer band of a disk), increasing the calculated permeabilities. The hemispherical model considers directly the surface area of mitigation pits in the hemispherical r_o term, which tends to reduce the calculated permeabilities.

Fits of Models: The fit of the experimental data to the non-linear permeability models (i.e., Equations 18-20) was considered in terms of an uncorrected correlation coefficient, r^2_{uncorr}, where

$$r^2_{uncorr} = \frac{\text{Uncorrected Sum of Squares for Regression}}{\text{Total Uncorrected Sum of Squares}} \qquad (24)$$

An r^2_{uncorr} value of unity corresponds to a perfect fit between the model and experimental data. The empirical fits to the spherical, hemispherical and cylindrical disk models were very good with r^2_{uncorr} values exceeding 0.99 in most cases.

Pressure Field Mapping: A preliminary analysis of induced subslab pressure fields in both pre- and post-mitigation time periods has been performed for the Oak Ridge study houses (see Table 4). The purpose was to examine mechanisms for expansion of induced pressure fields to enhance mitigation effectiveness, particularly in cases of low subslab permeability. The largest, postmitigation expansions were observed for measurement sites without a subslab gravel layer, where the premitigation permeabilities were lowest. For example, approximate one order of magnitude improvements were demonstrated for all measurement sites at House 16. This is consistent with the mathematical form of the hemispherical subslab model (Equation 21). The subslab air flow, Q, is proportional to r_o, the effective hemispherical radius of the volume of air across which minimal pressure drop occurs. The installation of 150 cm deep, loose gravel pits increased r_o by at least tenfold from approximately 2-5 cm to 65 cm. In contrast, the cylindrical disk model (i.e., Equation 22) is insensitive to variation in r_o. Consistent with this model, comparatively small improvements in pressure field radii are observed with the installation of gravel pits at measurement sites with a pre-existing gravel layer.

It should be emphasized that additional, substantive increases in r_o from those achieved in House 16 with 150 cm deep mitigation pits would have required massive excavations of soil from beneath the slab. In general terms, a hemispherical volume of soil (i.e., $0.67\ \pi\ r_o^3$) must be removed to achieve an effective hemispherical radius, r_o. In practice, larger and larger excavations become necessary to achieve only modest improvements in r_o. Future experiments will examine a multi-stage increase in both r_o and induced pressure in low permeability subslab media to verify these model developments.

Conclusions

Several tentative conclusions are drawn concerning the development of models describing the intrinsic permeability [(cm^2) per (cm H_2O/cm)] of soil and subslab media for radon diagnostic applications. Spherical, hemispherical and cylindrical disk models have been applied to permeability data taken in soil tubes, subslab soils without a distinct gravel layer, and subslab gravel layers, respectively. Collected numerical constants for the models differ from previously reported values by a factor of about 800 (2). This variation likely results from different interpretations of conductivity and permeability, and associated units conversions. A power dependence of approximately 0.7 was observed in all three models for the pressure term, confirming anticipated, non-laminar air flows. The hemispherical and cylindrical disk models predict that subslab air flow rates are proportional to the applied differential pressure$^{0.7}$, implying diminishing returns in mitigation effectiveness with increased blower capacity. The hemispherical model predicts a linear dependence on the effective hemispherical radius of a subslab hole, implying increased mitigation effectiveness with larger mitigation pits.

Numerous experimental data sets have demonstrated excellent fits to the above models. Interesting site-to-site, temporal and pre/post-mitigation variations in permeability are observed. Soil permeabilities taken in outdoor soil tubes surrounding the study homes show a combined 1000 fold variation with location and time. In contrast, subslab permeabilities commonly vary by twofold or less with time and location except in those homes with positionally distinct clay, soil or gravel subslab media. Particularly encouraging are the improvements in permeability and pressure field radii achieved with the installation of gravel-filled mitigation pits. The order of magnitude improvements observed in the low permeability subslab media present beneath House 16 greatly improve prospects for effective radon mitigation of such homes using subslab depressurization techniques.

References

1. D.T. Harrje, L.M. Hubbard, and D.C. Sanchez, PU/CEES Report No 223, Proceedings of the Radon Diagnostic Workshop, Princeton, NJ (April, 1987).

2. B. H. Turk, J. Harrison, R. J. Prill, and R. J. Sextro, Interim Report on Diagnostic Procedures for Radon Control. LBL-23089, Lawrence Berkeley Laboratory, Berkeley, CA (March, 1987).

3. B. S. Massey, Mechanics of Fluids, Van Nostrand Reinhold Company, New York, NY, 1975.

4. D.K. Todd, Groundwater Hydrology, Second Edition, John Wiley & Sons, New York, NY 1980.

5. T. G. Matthews, C. S. Dudney, K. P. Monar, D. C. Landguth, D. L. Wilson, A. R. Hawthorne, L. M. Hubbard, K. J. Gadsby, D. L. Bohac, C. A. Decker, A. M. Lovell, D. T. Harrje, and R. H. Socolow, Investigation of Radon Entry and Effectiveness of Mitigation Measures in Seven Houses in New Jersey: Midproject Report. ORNL/TM-10671, Oak ridge National Laboratory, Oak Ridge, TN, 1987.

6. M. Muskat, Physical Principles of Oil Production, McGraw-Hill Book Co., New York, NY 1949.

7. T. G. Matthews and C. S. Dudney, Quality Assurance/Project Plan: Investigation of Radon Entry and Effectiveness of Mitigation Measures in Eight Houses in the Tennessee Valley. Oak Ridge National Laboratory, Oak Ridge, TN, 1988.

8. SAS User's Guide: Statistics, 1982 ed; SAS Institute: Cary, N.C.

Table 1. Study design: house characteristics and intercomparisons

Parameter	Huntsville, AL				Oak Ridge, TN			
House	11	12	13	14	15	16	17	18
Substructure	(- - Crawlspace - - -)				(- Daylight Basement -)			
			(Bsmt/Garage)					
HVAC	(- - - - central forced air - - - - - -)						(ceil heat)	
Clustering	(- 0.25 mile radius -)				(- 0.75 mile radius -)			
Upstairs Area (ft^2)	1600	1500	2400	2100	1200	1800	1700	1800
Floor Levels	(Basement & Upstairs)				(Bsmt/Garage & Upstairs)			
Substructure Radon (pCi/L) 11-12/87	8	20	16	41	25	26	27	12

Table 2. Data Sheet for Subslab Diagnostic Communication Measurements

Investigator:_____ Date __/__/__ House #_____

Location of Hole:_____ 1.5" 4" 6" Depth:_____ Shape:_____

I. Flow vs Delta Pressure at Sampling Hole for Permeability

Delta Pressure (KPa)	Air Velocity (m/s)	Air Flow (l/min)	K (cm2)

II. Air Flow and Delta Pressure at Remote Locations

Induced DP	------ 5000 Pa -----		------ 2000 Pa -----		------ 500 Pa ------	
Remote Hole No. & Dist.	DP (In H2O)	Air Flow (m/s)	DP (In H2O)	Air Flow (m/s)	DP (In H2O)	Air Flow (m/s)
#						
#						
#						
#						
#						
#						
#						
#						
#						
#						
#						
#						
#						
#						

1 kPa = 10.2 cm H_2O || 1 m/s (1") = 31.86 l/m, (4") = 486.4 l/m, (6") = 1094 l/m

$$K\ (cm^2) = \frac{(4 \times 10^{-4} * \text{Velocity (m/sec)} * X\ \text{(l/min)/(m/sec)})}{(\text{Pressure}^{0.7}\ \text{(kPa)} * 10.2\ \text{(kPa/cm } H_2O) * \text{Radius (cm)}}$$

*** FOR PRELIMINARY CALCULATIONS ONLY ***

$K\ \underline{1.5"}(cm^2) = 6.6 \times 10^{-4} * \text{Velocity (m/sec)} / \text{Pressure}^{0.7}\ \text{(kPa)}$

$K\ \underline{4.0"}(cm^2) = 3.8 \times 10^{-3} * \text{Velocity (m/sec)} / \text{Pressure}^{0.7}\ \text{(kPa)}$

$K\ \underline{6.0"}(cm^2) = 5.6 \times 10^{-3} * \text{Velocity (m/sec)} / \text{Pressure}^{0.7}\ \text{(kPa)}$

Table 3. Intrinsic permeability (in 10^{-4} cm^2) of soil, and subslab media during pre- and post-mitigation conditions.

House	Soil Tube[a]	Slab Location	In Premitigation Diagnostic Holes At Depth Ranges (cm) 13-20	36-41	76-84	117-122	152	Mitigation Pit Depths (cm) 40	120
HU13	0.4-330	Gar.(Boat)[b]	14,14	130	110	130	-	-	-
		Gar. Center[b]	200,140 130	-	-	-	-	-	-
		Gar. Back[b]	110	-	-	-	-	110[d]	-
HU14	0.6-390	Gar. Back[b]	28,29	67,78	bedrock		-	97,95[d]	-
		Gar. Center[b]	67,68	93	104	bedrock	-	-	-
OR15	3.7-190	Closet[b]	120,75	85	80	82,117	-	260,250 350,320	-
		Work Room[c]	7.1,7.8	5.1	3.5	2.9,3.3	-	-	5.9,7.5 12,7.3
OR16	0.2- 35	Laundry[c]	.24,.29	.005	.15	.59,.60	.61, .69	-	2.8,3.2 8.4,5.8
		Den[c]	.14,.11	.081	.097	.12,.14	-	-	6.8,7.1 3.1,3.9
		Bedroom[c]	2.7,3.0	1.7	1.3	1.0,1.1	-	-	9.3,8.4 8.3,8.2
OR17	1.0-100	Work Room[b]	98,135	-	-	-	-	240,330 58	-
		Bathroom[b]	86,52	-	-	-	-	120,98	-
OR18	0.2- 20	Workshop[b]	210,180	-	-	-	-	380,400 430,360	-
		Fireplace[b]	160,200	-	-	-	-	310,260 420,300	-
		Front Wall[b]	120,150	-	-	-	-	-	-

[a] Calculated using the spherical model (i.e., Equation 18)

[b] Calculated using the cylindrical disk model (i.e., Equation 19)

[c] Calculated using the hemispherical model (i.e., Equation 20)

[d] Pit depth was 50 cm and 65 cm for HU13 and HU14, respectively.

Table 4. Semiquantitative analysis of maximum pressure field radii (cm), r_x, induced in pre- and post-mitigation experiments[a].

House	Sampling Location	Maximum Premitigation k (cm^2)	Premitigation Test Taken at 500 Pa	Post Mitigation at 320-400 Pa
OR15	Outdoor Closet	1.2 x 10-2	760	> 900
	Work Room	7.8 x 10-4	210 - 430[b]	> 1000
OR16	Laundry	6.9 x 10-5	< 75[b]	300 - 900
	Den Closet	1.4 x 10-5	< 25[b]	460 - 760
	Bedroom	3.0 x 10-4	75 - 120[b]	460 - 1200
OR17	Workroom	1.4 x 10-2	760	900
	Bathroom	8.6 x 10-3	900	460 - 900
OR18	Workshop	2.1 x 10-2	900	900 - 1200
	Fireplace	2.0 x 10-2	300 - 600	1200 - 1500

[a] Defined as >0.25 Pa induced differential pressure

[b] Estimated from pressure field measurements at 2000 Pa

Premitigation Diagnostic Subslab Application

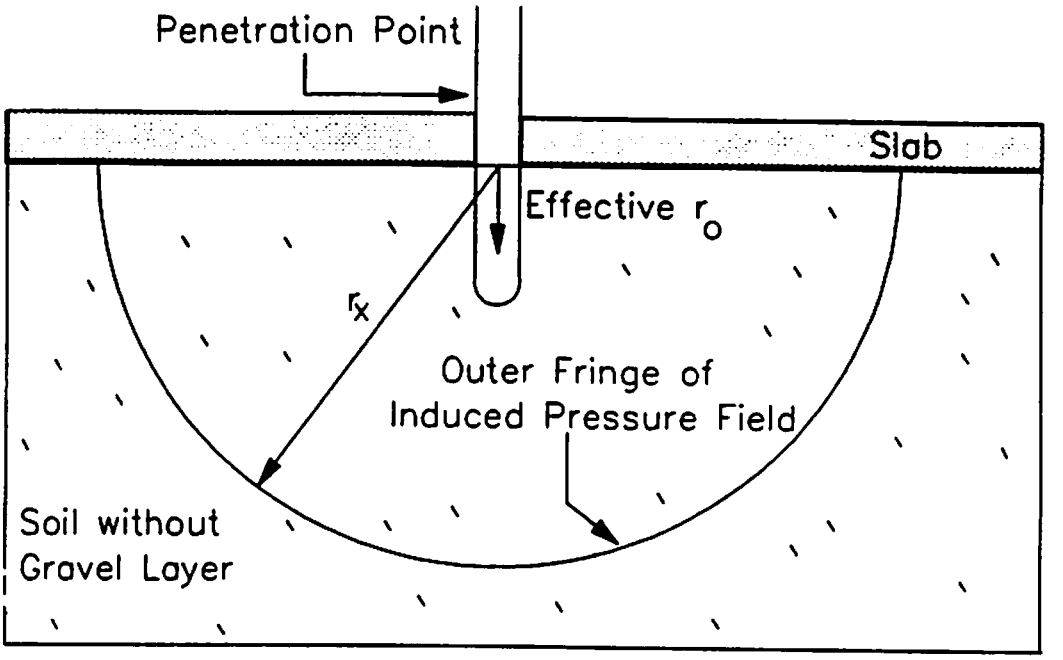

Postmitigation Diagnostic Application

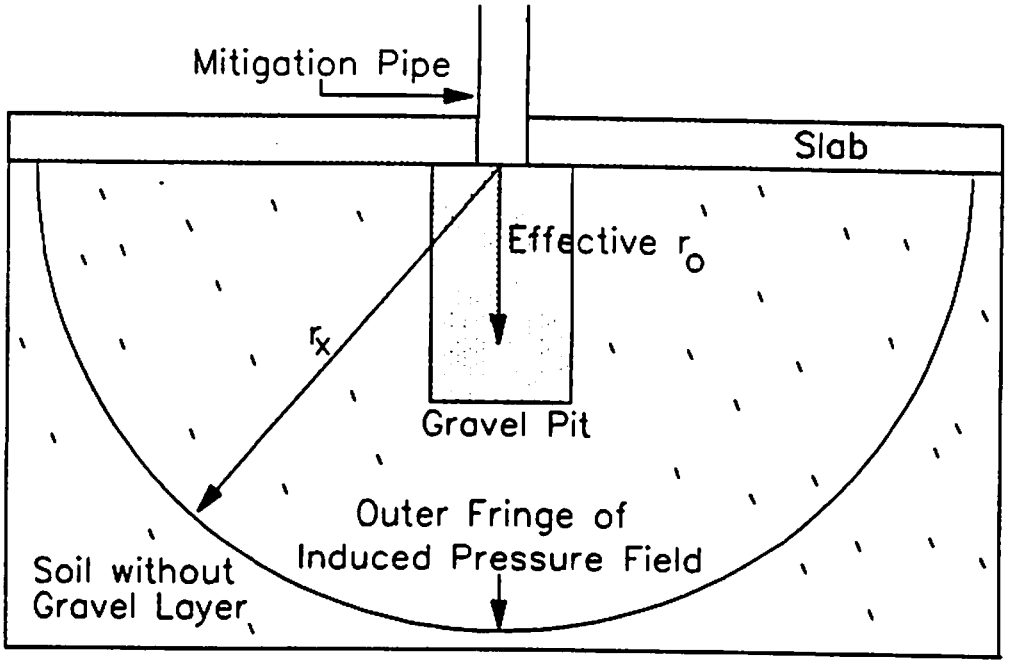

Figure 1: Hemispherical Model

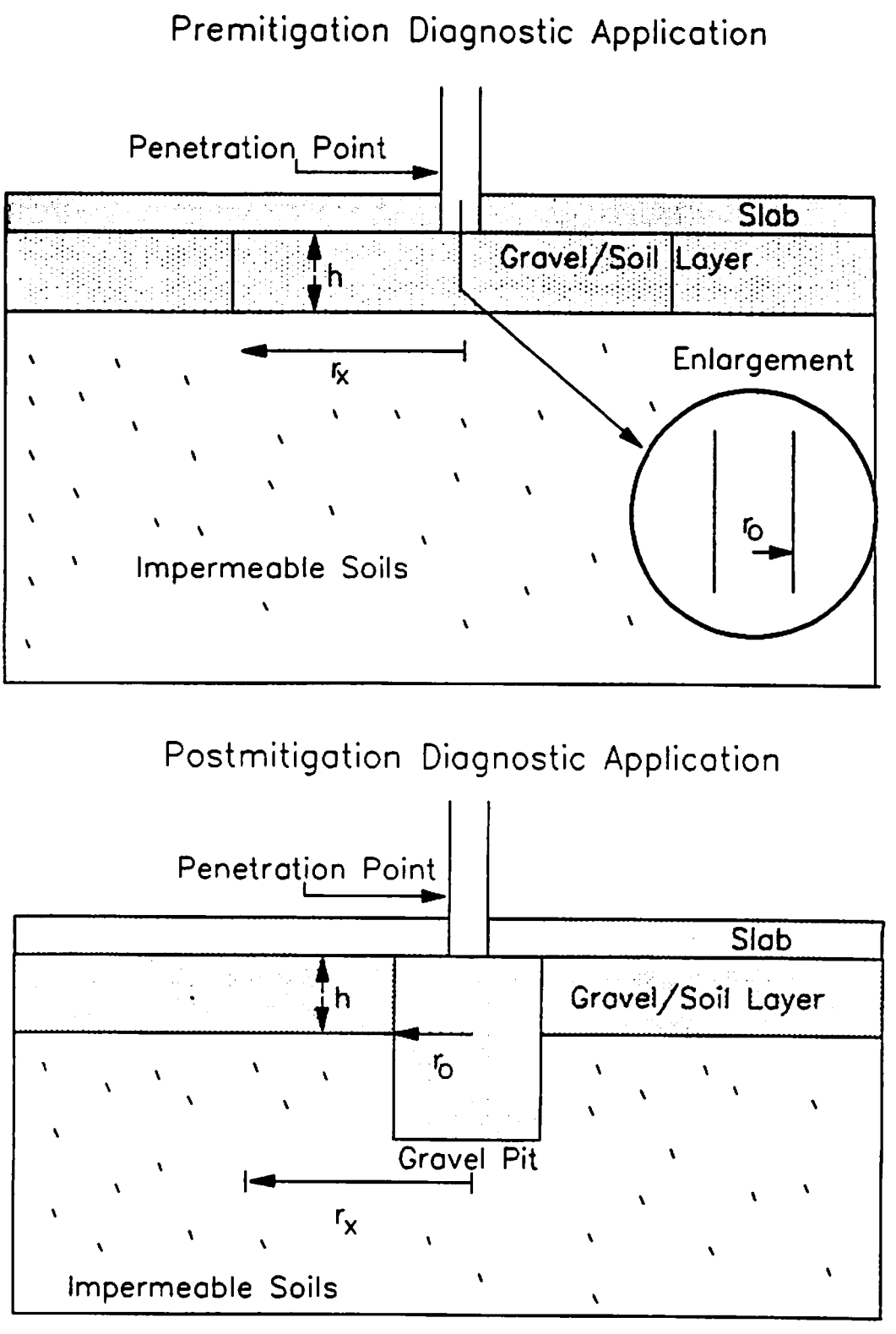

Figure 2: Cylindrical Disk Model